Nigerian Journal of Physics (NJP)
ISSN online: 3027-0936
ISSN print: 1595-0611
DOI: https://doi.org/10.62292/njp.v35(s).2026.723
Volume 35(S), 2026

Geophysical Investigation of Groundwater Contamination Risk and Radiological Assessment of Soil around Kurata Dumpsite, Southwestern Nigeria

*[1]Kamilu, M. A., [2]Coker, J. O., [2]Alausa, S. K., [2]Oladunjoye, H. T., [2]Adenuga, O. A., [2]Adekoya, S. O. and [3]Atilade, A. O.

[1]Department of Physical Sciences, Yaba College of Technology, Yaba, Lagos State, Nigeria.
[2]Department of Physics, Olabisi Onabanjo University, Ago-Iwoye, Ogun State, Nigeria.
[3]Department of Physical Sciences, Lagos State University of Science and Technology, Ikorodu, Lagos State, Nigeria.

*Corresponding Author's Email: kamiladeshina@gmail.com

Keywords:
Dumpsite,
Geophysical,
Leachate,
Protective capacity,
Radiological,
Resistivity.

Submitted: 10 Jun. 2026

Accepted: 16 Aug. 2026

Published: 8 Sep. 2026

ABSTRACT
Inadequate solid waste management can lead to groundwater contamination and radiological pollution. This study assessed subsurface conditions, groundwater vulnerability, and radiological health risks at the Kurata dumpsite using integrated geophysical and radiological methods. Fifteen 2D electrical resistivity imaging traverses and Vertical Electrical Sounding (VES) surveys were conducted to characterize the subsurface and evaluate the protective capacity of overburden materials. The results identified subsurface layers consisting of topsoil, peat/leachate, clay, clayey sand, sand, and dry sand. Low-resistivity zones (<15 Ωm) indicated leachate accumulation and possible contaminant migration, especially in areas where the protective clay layer was thin or absent. Longitudinal conductance values ranged from 0.0503 to 0.938 mho, indicating poor to good protective capacities across the site. Radiological analysis showed that the mean activity concentrations of ^{40}K, ^{238}Ra, and ^{232}Th were within internationally accepted background levels. Radiological hazard indices, annual effective dose, and excess lifetime cancer risk were all below recommended safety limits, indicating minimal radiological risk. Correlation analysis revealed a weak to moderate relationship between topsoil resistivity and radionuclide concentrations, with K-40 showing the strongest association, while Ra-226 exhibited very little correlation. The low correlation coefficients suggest that radionuclide distribution is influenced by factors such as lithology, weathering, mineral composition, and environmental conditions rather than resistivity alone. Overall, while leachate may threaten groundwater quality, radiological risks remain low, highlighting the need for continuous environmental monitoring and improved waste management practices.

INTRODUCTION

Poor management of solid waste poses significant environmental and public health challenges, particularly through groundwater contamination and the spread of infectious and waterborne diseases (Adewuyi *et al*., 2014; Adebayo *et al*., 2015). In addition to generating unpleasant odors and harboring pathogenic microorganisms, dumpsites may also contain radioactive materials capable of contributing to environmental radiation exposure. Previous studies have reported measurable concentrations of naturally occurring radionuclides in vegetation and other environmental media in Nigeria (Akinloye & Olomo, 2005), highlighting the need to assess radiological conditions around waste disposal sites.

Geophysical methods, including electrical resistivity, seismic, electromagnetic, and magnetic techniques, have been widely applied in environmental investigations. These methods have proven effective for landfill and dumpsite characterization, delineation of contaminant plumes, and assessment of the extent of subsurface pollution (Ehirim *et al*., 2009; Fajana, 2013; Olagunju *et al*., 2017). Among these techniques, electrical resistivity surveying is particularly valuable because it provides rapid, cost-effective, and reliable information on subsurface lithology, groundwater conditions, and contaminant migration pathways. Consequently, it is widely used to evaluate the hydrogeological characteristics of dumpsites and their potential impacts on groundwater resources.

The hydrogeological setting plays a critical role in controlling the movement of leachate generated from waste disposal sites. Low-permeability geological units, commonly referred to as aquitards, aquicludes, or aquifuges, act as natural barriers that restrict the downward migration of contaminants into underlying aquifers (Stempvoort *et al*., 1992; Yusuf *et al*., 2019; Obiora *et al*., 2020). Conversely, where these protective layers are thin, fractured, or absent, leachate can infiltrate more readily, increasing the vulnerability of groundwater resources. In this study, the geoelectrical resistivity method was employed to determine subsurface stratigraphy, estimate aquifer thickness, and evaluate the protective capacity of the overburden, thereby assessing the susceptibility of groundwater to contamination.

Radiological assessment is equally important for evaluating the environmental quality of dumpsites and the potential exposure of nearby residents and workers. Such assessments involve determining the concentrations of naturally occurring radionuclides in environmental media, including soil, water, and air, and estimating associated exposure pathways through inhalation and ingestion (Olubunmi *et al*., 2018). Evaluating natural background radioactivity and its radiological implications is essential for protecting both human health and the environment from radiation hazards (Kasoga *et al*., 2015). Natural background radiation originates primarily from two sources: high-energy cosmic radiation and naturally occurring radionuclides present in the Earth's crust, which are ubiquitous in the environment and contribute to normal human radiation exposure (United Nations Scientific Committee on the Effects of Atomic Radiation [UNSCEAR], 2000).

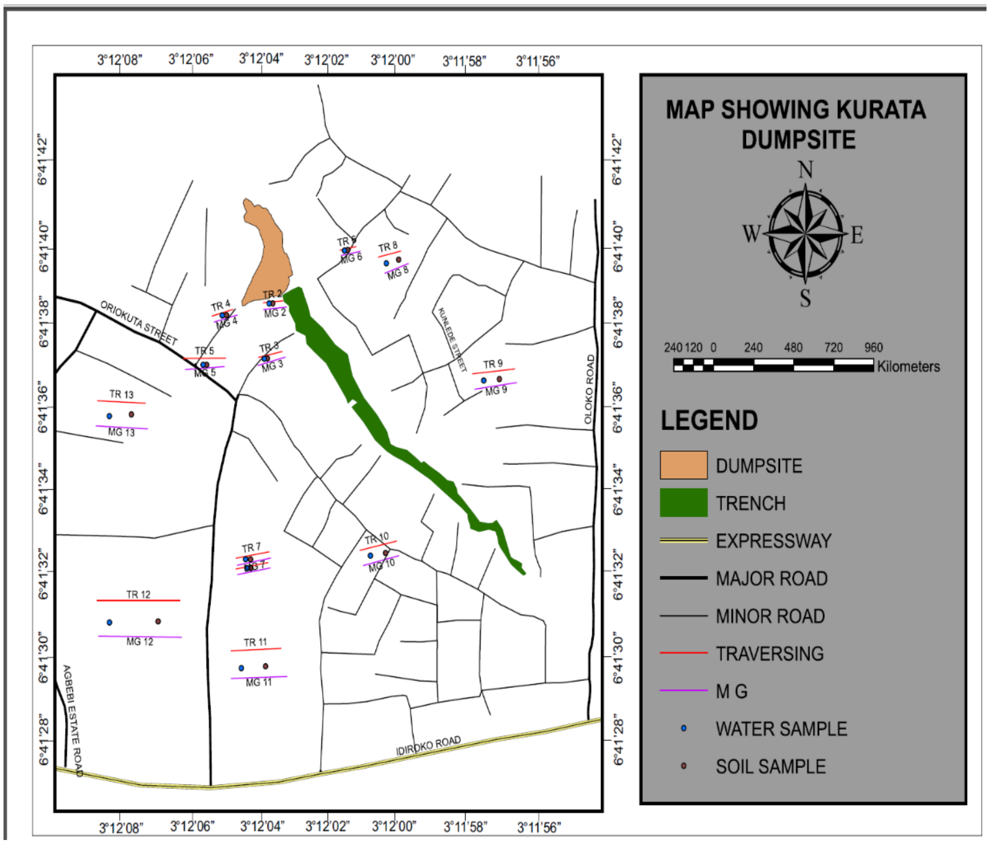

Plate 1: Base Map of Kurata Dumpsite, Ado-Odo Ota, Ogun State

Geology of Study Area

Ota (Sango-Ota), located in Ado-Odo/Ota Local Government Area of Ogun State, lies within the eastern margin of the Dahomey Basin, where the Precambrian Basement Complex transitions into younger sedimentary formations. This geological setting plays a significant role in groundwater occurrence, aquifer characteristics, and the movement of contaminants from surface sources such as dumpsites (Jones & Hockey, 1964; Kogbe, 1976).

The Basement Complex consists mainly of granite gneiss, migmatite, porphyritic granite, and biotite granite. These crystalline rocks have low primary porosity, with groundwater occurring mainly within weathered and fractured zones, making such areas susceptible to contaminant infiltration where the overburden is thin (Rahaman, 1988).

The sedimentary sequence comprises the Abeokuta, Ewekoro, Oshosun, Ilaro, and Benin Formations (Coastal Plain Sands), which consist of sands, sandstone, clay, shale, limestone, and gravel. The highly permeable Benin Formation serves as the principal aquifer, providing substantial groundwater storage but also increasing the potential for leachate migration from poorly managed dumpsites. In contrast, clay-rich horizons within the Oshosun Formation may act as protective barriers that limit contaminant movement (Omatsola & Adegoke, 1981).

Overall, the geological and lithological characteristics of Ota are important for understanding groundwater vulnerability and interpreting geophysical investigations of dumpsite impacts on groundwater quality, as shown in figure 2.

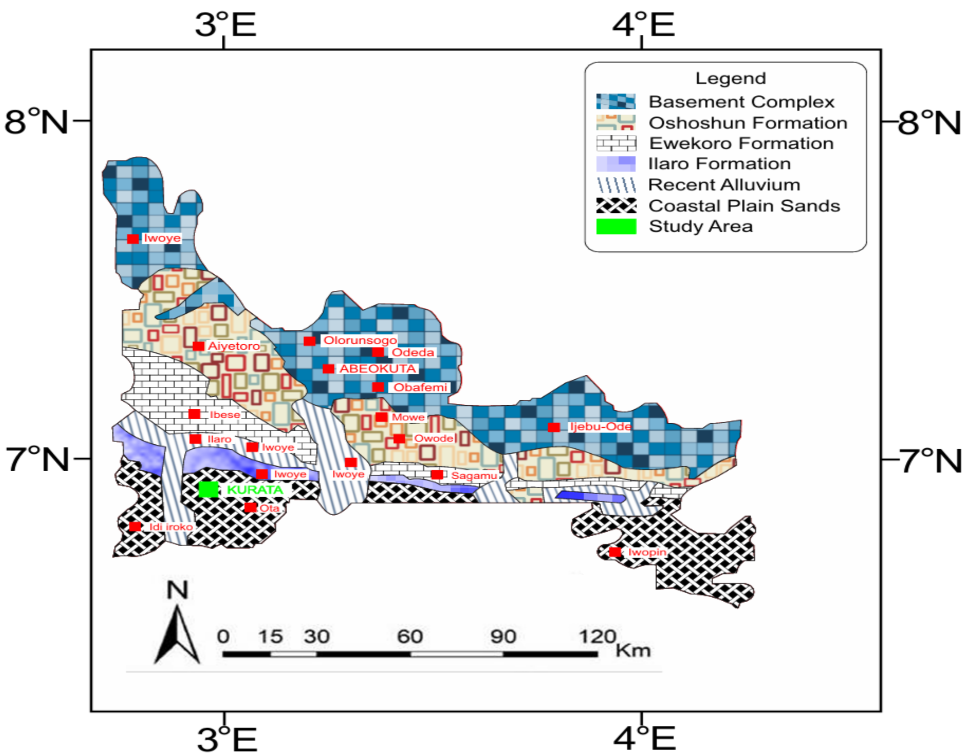

Plate 2: Geology Map of Ogun State (Modified from Coker *et al*., 2013)

MATERIALS AND METHODS

2D Wenner Field Procedure and Processing

A 2D geoelectrical resistivity survey was conducted using the Wenner array configuration and an OHM Earth Resistivity Meter, together with metal electrodes, conducting cables, and hammers. Data were collected along 15 profiles, each 200 m long, with electrodes spaced at 5 m intervals. Apparent resistivity measurements were obtained from multiple electrode combinations through manual switching, enabling the investigation of both vertical and lateral variations in subsurface resistivity. The collected data were formatted and processed using RES2DINVx64 software. The software applies finite-difference or finite-element inversion algorithms to convert apparent resistivity measurements into true subsurface resistivity models by iteratively minimizing the difference between measured and calculated values. The resulting 2D resistivity sections provide detailed images of subsurface resistivity distribution, revealing both vertical and lateral changes. These sections were interpreted to delineate lithological boundaries, identify groundwater-bearing zones, detect structural features, and map potential contamination pathways across the study area

1D Vertical Electrical Sounding (VES) Field Procedure and Processing

A Vertical Electrical Sounding (VES) survey was conducted using the Schlumberger electrode array and an OHM Earth Resistivity Meter, together with metal electrodes, connecting cables, and hammers. In this configuration, four electrodes were arranged symmetrically along a straight line, with the current electrodes positioned outside the potential electrodes (AB/2 ≥ MN/2). To investigate greater depths, the spacing of the current electrodes (AB/2) was progressively increased while the potential electrodes remained relatively fixed, reducing field effort since only the current electrodes required frequent repositioning. A total of 30 VES stations were occupied at each dumpsite. The 1D resistivity survey was designed to determine the variation of subsurface electrical resistivity with depth and identify the thickness and resistivity of underground layers. Field data were processed using WinResist software, which applies curve matching and inversion techniques to estimate the true resistivity and thickness of subsurface layers. The resulting layered resistivity models were interpreted and correlated across the study area to characterize subsurface conditions and assess groundwater and geological features.

Aquifer Vulnerability Index (AVI)

The Aquifer Vulnerability Index (AVI) method, developed by Van Stempvoort *et al.* (1993), evaluates the degree of protection provided by geological materials overlying an aquifer. The method considers two primary parameters: the thickness of the protective layer and its hydraulic conductivity. Using these parameters, the hydraulic resistance of the protective Rating can be calculated. A thicker protective layer with low hydraulic conductivity provides greater resistance to contaminant movement and therefore indicates lower aquifer vulnerability. The protective layer above an aquifer may be described as an aquitard, aquiclude, or aquifuge. In urban environments where vertical contaminant infiltration is common, evaluating the protective capacity of these layers is particularly important as shown in Table 1.

Table 1: Longitudinal Conductance, Groundwater vulnerability Level and Protective Capacity Stempvoort *et al.* (1993)

Longitudinal (mhos)	Conductance Vulnerability Level	Protective Capacity Rating
>10	Very Low	Excellent
5-10	Low	Very Good
0.7-4.9	Moderate	Good
0.2-0.69	High	Moderate
0.1-0.19	Very High	Weak
<0.1	Extremely High	Poor

Radiological Materials and Methods

A total of thirty (30) soil samples were collected at fifteen (15) different points from the selected dumpsite of different districts' areas near the dumpsite using the hand auger after careful removal of overlying waste. The soil samples were taken at 0.5 and 1.0 m depth of each transect by the use of the hand-driven auger, and the GPS coordinates were taken. The collected soil samples are taken to the laboratory in labeled polyethylene bags for further analyses. We made sure to clean the auger after each sample collection.

Stones and organic matter were first removed from each sample so as to expose the soil at each sampling point (each of these samples weighs about 1.5 kg). The samples were dried by placing them in the oven at 110 °C for about 24 hr. They were then pulverized (reduced to fine particles) and filtered through a 2 mm mesh sieve. We endeavor to clean the mesh after every sieve to avoid cross-contamination. The homogenized soil samples were sealed in plastic containers and left there for at least one month, before gamma spectrometric analysis, to attain a secular equilibrium.

After attaining the secular equilibrium, the soil samples were then analyzed for 10 hours using gamma ray spectrometry analysis of the soil samples for natural radioactivity; this was carried out using a NaI(Tl) detector. The detector was interfaced to a PC computer with a program installed for this purpose to make it equivalent to a multi-channel analyzer. The system also contains the usual electronic components of a preamplifier, amplifier, and power supply.

Radiological health parameters were calculated with the mathematical formula, and the results were compared with UNSCEAR, 2020, as shown in Table 2.

Table 2: Word average values, UNSCEAR, 2020

S/N	Radiological health hazard parameters	Mathematical formula	Units	World average value (UNSCEAR, 2020)
1.	Absorbed Dose Rate(Dr)	$D^R = 0.46Au + 0.604ATh + 0.0417Ak$	$NGyhr^{-1}$	57
2.	Radium equivalent(Raeq)	$Ra_{eq} = AU + 1.43Th + 0.077Ak$	$Bq\ kg^{-1}$	370
3.	Annual effective dose equivalent ($AEDE_{outdoor}$)	AEDE(outdoor) = DR(nGhr-1)×8766hr×0.7SvG − 1 ×0.2×10-3	$(\mu Svyr^{-1})$	70
4.	Annual effective dose equivalent($AEDE_{indoor}$)	AEDE(indoor) = D_R ($nGyhr^{-1}$) ×8766 hr × 0.7 SvG^{-1} × 0.8 × 10^{-3}	$(\mu Svyr^{-1})$	450
5.	External Hazard index(Hext)	$H_{ext} = \frac{AU}{370} + \frac{ATh}{259} + \frac{Ak}{4810} \leq 1$		≤ 1
6.	Internal Hazard index(Hint)	$H_{ext} = \frac{AU}{185} + \frac{ATh}{259} + \frac{Ak}{4810} \leq 1$		≤ 1
7.	External(y-radioactivity) level index	$H_{yr} = \frac{AU}{300} + \frac{ATh}{200} + \frac{Ak}{300}$		≤ 0.5
8.	Activity utilization index(AUI)	$AUI = ((\frac{AU}{500Bqkg})\ fk \leq 2$		≤2
9.	Exposure Rate(ER)	$ER = 1.90Au + 4.18\ A_{Th} + 0.315\ A_k$	(μRhr^{-1})	600
10.	Annual gonadal dose equivalent(AGDE)	$AGDE = 3.09\ AU + 4.18Th + 0.315A_k$	$(\mu Svyr^{-1})$	1000
11.	Excess Life Time Cancer Risk(ELCR) outdoor	$ELCR_{(outdoor)} – AEDE_{(outdoor)}$ DL × RF	$(\mu Svyr^{-1})$	0.29

RESULTS AND DISCUSSION

Interpretation of 2D Resistivity Sections

Figure 1 presents the 2D resistivity image of the subsurface beneath Traverse One, which spans a total length of 100 m with an investigated maximum depth of 19.8 m. The resistivity values along the profile range from 10.1 to 197 Ω·m. Five distinct geoelectric layers were delineated, comprising topsoil, peat/leachate, clay, clayey sand, and sand. The topsoil layer, consisting of a mixture of clay and peat/leachate, has a thickness ranging from 0 to 1.25 m across the profile, with resistivity values between 10.1 and 15.4 Ω m. Beneath this layer, peat/leachate zones extend to depths of approximately 1.25–6.28 m and 6.28–9.26 m. These zones are characterized by very low resistivity values (<15 Ω m), indicative of leachate contamination, with values fluctuating between 1.83 and 5.87 Ω m (Adewole, 2009; Raji & Adeoye, 2017). The clay layer occurs as a relatively thin unit across the profile at a depth of about 12.4 m, with resistivity values ranging from 22.6 to 55.1 Ω m. This is underlain by a clayey sand layer, also thin and laterally continuous, with a resistivity value of approximately 84.2 Ω m at a depth of 15.9 m. The deepest geoelectric unit is sand, exhibiting resistivity values between 129 and 197 Ω m at depths ranging from 15.9 to 19.4 m.

Figure 2 shows the 2D resistivity image beneath Traverse Two, which also covers a length of 100 m with a maximum investigated depth of 19.8 m. The resistivity values along this profile range from 11 to 772 Ω m. Six geoelectric layers were identified, including topsoil, peat/leachate, clay, clayey sand, sand, and dry sand. The topsoil layer, composed of clay mixed with peat/leachate, has a thickness of 0–1.25 m and resistivity values ranging from 11 to 20.1 Ω m. The underlying peat/leachate layer extends from depths of approximately 1.25 to 6.38 m and is marked by very low resistivity values (<15 Ω m), consistent with leachate-saturated materials (Adewole, 2009; Ameloko & Ayolabi, 2018). The clay layer, forming the second geoelectric unit, has resistivity values ranging from 37.0 to 67.9 Ω m and occurs between depths of 6.38 and 9.26 m. This is followed by a thin clayey sand layer with an average resistivity of about 125 Ω m at a depth of approximately 10.0 m. The fourth layer consists of sand with a resistivity value of about 229 Ω m, occurring between depths of 10.0 and 12.4 m. The deepest layer is dry sand, characterized by high resistivity values ranging from 420 to 772 Ω m at depths between 15.9 and 19.4 m across the profile.

Figure 3 illustrates the 2D resistivity image of the subsurface beneath Traverse Three, extending over a length of 100 m with a maximum depth of 19.8 m. The resistivity values along this profile range from 31.5 to 537 Ω·m. Five geoelectric layers were identified: topsoil, clayey sand, sandy clay, sand, and dry sand. The topsoil layer, comprising clay and clayey sand, has a thickness ranging from 0 to 3.75 m and resistivity values between 31.6 and 106 Ω m. The second layer, consisting of clayey sand, extends from depths of approximately 3.75 to 6.28 m across the profile. Beneath this, the third layer identified as sandy clay exhibits resistivity values ranging from 106 to 159 Ω m at depths between 6.38 and 9.26 m. The fourth layer is a relatively thin sand unit occurring across the profile, with resistivity values ranging from 239 to 358 Ω m at a depth of about 12.4 m. The fifth layer consists of sand and dry sand, characterized by resistivity values between 358 and 537 Ω m at depths around 15.9 m. The deepest geoelectric unit is sand, with resistivity values ranging from 129 to 197 Ω m at depths between 15.9 and 19.8 m across the profile.

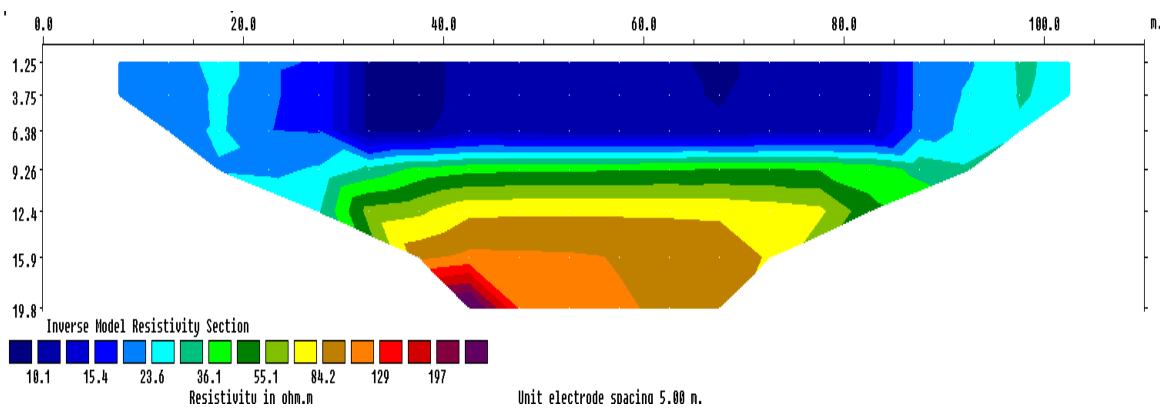

Figure 1: 2-D resistivity pseudo-section along Traverse One

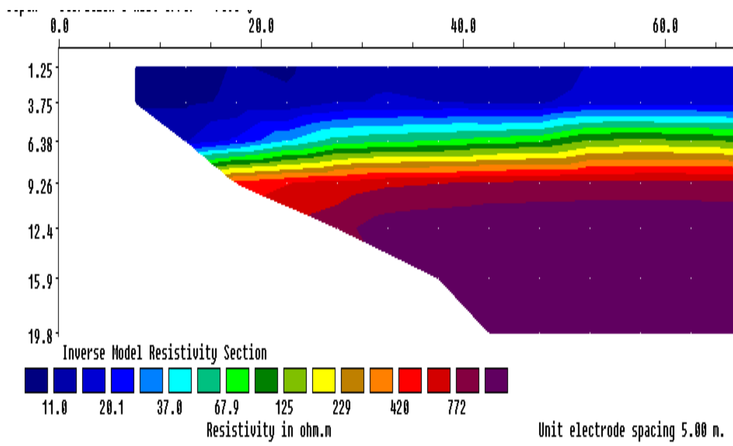

Figure 2: 2-D Resistivity Pseudo-Section along Traverse Two

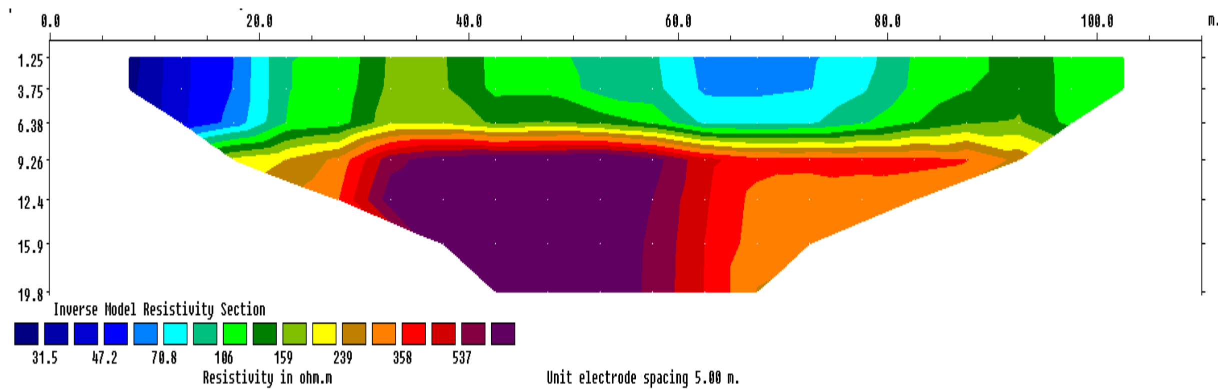

Figure 3: 2-D Resistivity pseudo Section along Traverse Three

Aquiver Vulnerability Results

The Vertical Electrical Sounding (VES) data reveal variations in subsurface lithology and aquifer protective capacity across the study area. The longitudinal conductance (S) values were used to assess the protective capacity of the overburden against contaminant infiltration. Five geoelectric layers were identified: topsoil (18.9 Ω m, 0.6 m), peat/leachate-contaminated layer (9.64 to 14 Ω m), clay (24.4 to 100 Ω m), and sandy clay (185 Ω m) and sand (200 – 360 Ωm). The low resistivity of the second layer suggests the presence of leachate infiltration. However, the thick clay layer provides significant attenuation of contaminants. The longitudinal conductance value of 0.0169 to 0.9382 mho indicates a poor, weak, and good protective capacity of the Study area.

Table 3: Kurata Vulnerablilty Results

Traverse	Long.	Lat.	Lays	Res.(Ω m)	Thick (m)	Lithology	Long. C.layer	Interpretation
1.3°	11'57.84"	6°41'12.58"	1	18.9	0.6	Top soil	0.723655	Good protective layer
			2	9.64	7.27	Peat/leachate		
			3	24.4	19.3	Clay		
			4	185	Sandy clay			
2.3°	11'59.75"	6°41'31.01"	1	8.81	0.57	Top soil	0.86298	Good protective layer
			2	2.33	2.43	Clay infiltrated leachate		
			3	32.9	24.5	Clay		
			4	360	Sand			
	1	4.19	1.27	Top soil				
3.3°	11'55.97"	6°41'30.11"	1	96	1.31	Top soil	0.283646	weak protective layer
			2	31.4	9.76	Clay		
			3	178	16.6	Sandy clay		
			4	726	Lateritic sand			
4.3°	11'54.30"	6°41'26.77"	1	10	1.46	Top soil	0.188909	weak protective layer

			2	55	3.82	Clay		
			3	854	17.9	Lateritic sand		
			4	434	Sand			
5.3°	12'05.95"	6°41'34.75"	1	49.9	1.19	Top soil	0.062805	Poor protective layer
			2	90.4	5.59	Clayey sand		
			3	328	26.2	Sand		
			4	184	Sandy clay			

Discussion of Radiological Analysis

Table 4a: Kurata Radiological Results

Sample Points	K-40	U-238	Th-232	K-40	U-238	Th-232
TR1(0.5)	397.82 ± 10.18	13.26 ± 1.42	8.24 ± 0.56	397.82	13.26	8.24
TR1(1.0)	401.75 ± 8.15	15.23 ± 1.52	10.04± 1.85	401.75	15.23	10.04
TR2(0.5)	442.51 ± 7.56	15.82 ± 1.34	7.93 ± 0.61	442.51	15.82	7.93
TR2(1.0)	464.63 ± 7.15	`15.03 ±1.41	8.33±0.64	464.63	15.07	8.33
TR3(0.5)	428.49 ± 9.52	18.24 ± 1.63	8.58 ± 1.01	428.49	18.24	8.58
TR3(1.0)	449.92±9.99	19.15±1.71	9.01±1.10	449.92	19.15	9.01
TR4(0.5)	386.62 ± 8.76	12.64 ± 1.59	8.13 ± 0.96	386.62	12.64	8.13
TR4(1.0)	579.93±9.19	13.27±1.67	8.56±1.01	579.93	13.27	8.56
TR5(0.5)	486.87 ± 13.15	12.36 ± 1.46	10.32 ± 1.16	486.87	12.36	10.32
TR5(1.0)	511.21±13.80	12.97±1.53	10.84±1.22	511.2	12.97	10.84
TR6(0.5)	474.29 ± 12.81	13.45 ± 1.32	7.36 ± 0.58	474.29	13.45	7.36
TR6(1.0)	498.01±13.45	14.12±1.38	7.73±0.61	498.26	14.12	7.73
TR7(0.5)	518.41 ± 10.61	12.93 ± 1.64	8.31 ± 1.45	518.41	12.93	8.31
TR7(1.0)	544.33±11.14	13.57±1.72	8.73±1.52	544.33	13.57	8.73
TR8(0.5)	492.58 ± 10.34	11.97 ± 1.75	10.08 ± 1.21	492.58	11.97	10.08
TR8(1.0)	517.21±10.86	12.56±1.84	10.58±1.27	517.21	12.56	10.58
TR9(0.5)	396.63 ± 8.42	10.42 ± 1.08	8.42 ± 0.35	396.63	10.42	8.42
TR9(1.0)	416.46±8.84	10.94±1.13	8.84±0.36	416.46	10.94	8.84
TR10(0.5)	437.67± 9.36	12.11 ± 1.62	10.02 ± 1.17	437.67	12.11	10.02
TR10(1.0)	459.55±9.83	12.72±1.70	5.02±1.23	459.55	12.72	5.02
TR11(0.5)	456.77 ± 13.25	11.39 ± 1.36	10.52 ± 1.26	456.77	11.39	10.52
TR11(1.0)	479.61±13.91	11.96±1.43	11.05±1.32	479.61	11.96	11.05
TR12(0.5)	480.22 ± 12.61	13.25 ± 1.32	7.46 ± 0.48	480.22	13.25	7.46
TR12(1.0)	504.23±13.24	13.91±1.38	7.83±0.50	504.23	13.91±1.38	7.83
TR13(0.5)	548.61 ± 10.61	11.14 ± 1.64	8.61 ± 1.55	548.61	11.14	8.61
TR13(1.0)	576.04±11.14	11.69±1.72	9.04±1.63	576.04	11.69	9.04
Dumpsite1(0.5)	462.88 ± 10.42	11.85 ± 1.75	10.48 ± 1.36	462.88	11.85	10.48
1	486.02±10.94	12.44±1.83	11.00±1.43	486.02	12.44	11
Dumpsite2(0.5)	392.64 ± 10.26	12.41 ± 1.22	8.55 ± 0.62	392.64	12.41	8.55
2	412.27±10.77	13.03±1.28	8.97±0.65	412.27	13.03±1.28	8.97

Table 4b: Kurata Radiological Results

Sample Point	AEDEout	AEDEin	Hex	Hin	AGDE	ELCRout	ER
TR1(0.5)	33.92916	135.7166	0.150607	0.186445	87.94793	118.7521	184.9505
TR1(1.0)	36.57485	146.2994	0.163752	0.204914	101.683	128.012	197.4555
TR2(0.5)	37.42922	149.7169	0.165611	0.208367	95.97027	131.0023	202.5961
TR2(1.0)	38.43365	153.7346	0.169739	0.210469	96.02155	134.5178	209.8109
TR3(0.5)	38.55894	154.2358	0.171766	0.221063	105.7234	134.9563	205.4948
TR3(1.0)	40.48678	161.9471	0.180354	0.23211	111.0078	141.7037	215.7716
TR4(0.5)	32.92513	131.7005	0.146175	0.180337	85.21953	115.238	179.7847
TR4(1.0)	43.4851	173.9404	0.18974	0.225605	95.0529	152.1979	243.6718
TR5(0.5)	39.51627	158.0651	0.174781	0.208187	96.66641	138.307	219.9857
TR5(1.0)	41.48985	165.9594	0.183512	0.218566	101.4913	145.2145	230.9822
TR6(0.5)	37.29523	149.1809	0.163594	0.199946	87.26544	130.5333	205.7212
TR6(1.0)	39.17313	156.6925	0.171828	0.209991	91.63739	137.106	216.0913

TR7(0.5)	39.96192	159.8477	0.175058	0.210004	91.01942	139.8667	222.602
TR7(1.0)	41.95966	167.8386	0.183811	0.220487	95.5691	146.8588	233.7384
TR8(0.5)	39.41049	157.642	0.173981	0.206332	94.63797	137.9367	220.0401
TR8(1.0)	41.37331	165.4932	0.182641	0.216587	99.32692	144.8066	231.0096
TR9(0.5)	32.39947	129.5979	0.143384	0.171546	79.88725	113.3981	179.9321
TR9(1.0)	34.01806	136.0722	0.150547	0.180114	83.87429	119.0632	188.9221
TR10(0.5)	36.63688	146.5475	0.16271	0.195439	93.09011	128.2291	202.7587
TR10(1.0)	34.39625	137.585	0.149452	0.18383	74.76423	120.3869	189.9099
TR11(0.5)	37.57786	150.3115	0.16668	0.197464	93.55696	131.5225	209.4972
TR11(1.0)	39.46008	157.8403	0.175031	0.207356	98.25312	138.1103	219.9902
TR12(0.5)	37.55974	150.239	0.164676	0.200487	87.25223	131.4591	207.6271
TR12(1.0)	39.43405	157.7362	0.172891	0.210486	91.59455	138.0192	217.9909
TR13(0.5)	40.71878	162.8751	0.177666	0.207774	87.69362	142.5157	229.968
TR13(1.0)	42.75038	171.0015	0.186529	0.218123	92.05456	149.6263	241.4508
Dumpsite1	38.12021	152.4808	0.169038	0.201065	95.00362	133.4207	212.1286
1	40.02164	160.0866	0.177467	0.211088	99.72923	140.0758	222.7123
Dumpsite2	33.41436	133.6574	0.148439	0.18198	86.45406	116.9502	182.9996
1	35.07913	140.3165	0.15583	0.191046	90.74381	122.777	192.1167

The measured activity concentrations of natural radionuclides at the Kurata dumpsite indicate spatial variation across the investigated traverses. The activity concentration of ^{238}Ra ranged from a minimum value of 10.42 ± 1.00 Bq kg^{-1} at Traverse 5 to a maximum value of 19.10 ± 1.17 Bq kg^{-1} at Traverse 3. Similarly, the activity concentration of ^{232}Th varied from 7.36 ± 0.58 Bq kg^{-1} at Traverse 6 to 19.15 ± 1.17 Bq kg^{-1} at Traverse 14, which is located within the dumpsite. For ^{40}K, the minimum activity concentration of 386 ± 8.76 Bq kg^{-1} was observed at Traverse 5, while the maximum value of 576 ± 11.14 Bq kg^{-1} occurred at Traverse 13. The mean activity concentrations of ^{40}K, ^{238}Ra, and ^{232}Th across all analyzed samples were 397.82 ± 30.05 Bq kg^{-1}, 13.26 ± 3.01 Bq kg^{-1}, and 8.24 ± 2.20 Bq kg^{-1}, respectively, as illustrated in Figure 4. These values are generally within the typical global background levels reported for soils, although localized enrichment—particularly of ^{40}K—may be attributed to anthropogenic inputs such as domestic waste, construction debris, and organic matter accumulation within the dumpsite.

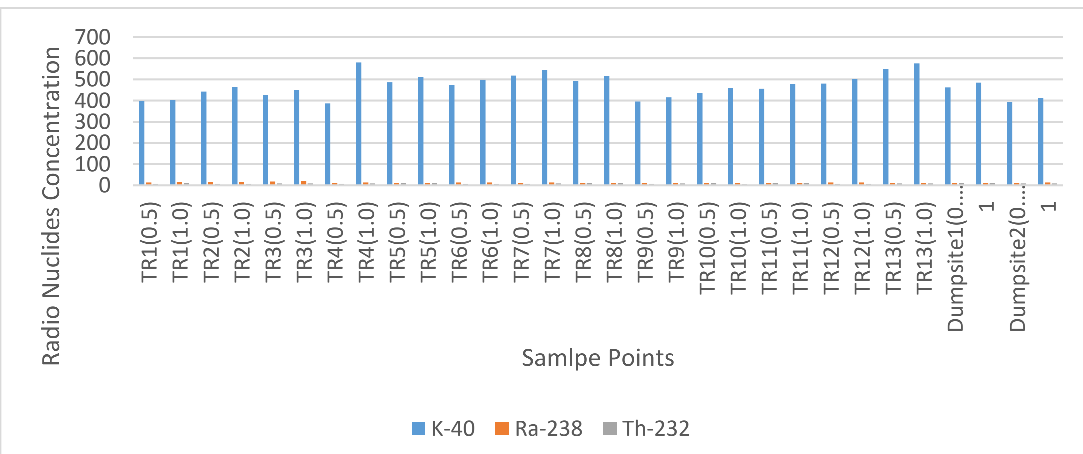

Figure 4: Radio Nuclide concentration VS Sample Points

The calculated radium equivalent activity (Ra_eq**)**, which provides a single index to assess the combined radiological hazard of ^{238}Ra, ^{232}Th, and ^{40}K, ranged from 53.00 Bq kg^{-1} to 70.17 Bq kg^{-1}, with a mean value of 55.67 Bq kg^{-1}. These values are significantly lower than the recommended maximum permissible limit of 370 Bq kg^{-1} for materials used by the public (Ugwuanyi *et al.*, 2021). This suggests that the soils within the study area do not pose significant radiological hazards. Figure 4e illustrates the spatial distribution of radium equivalent activity across the sampling locations.

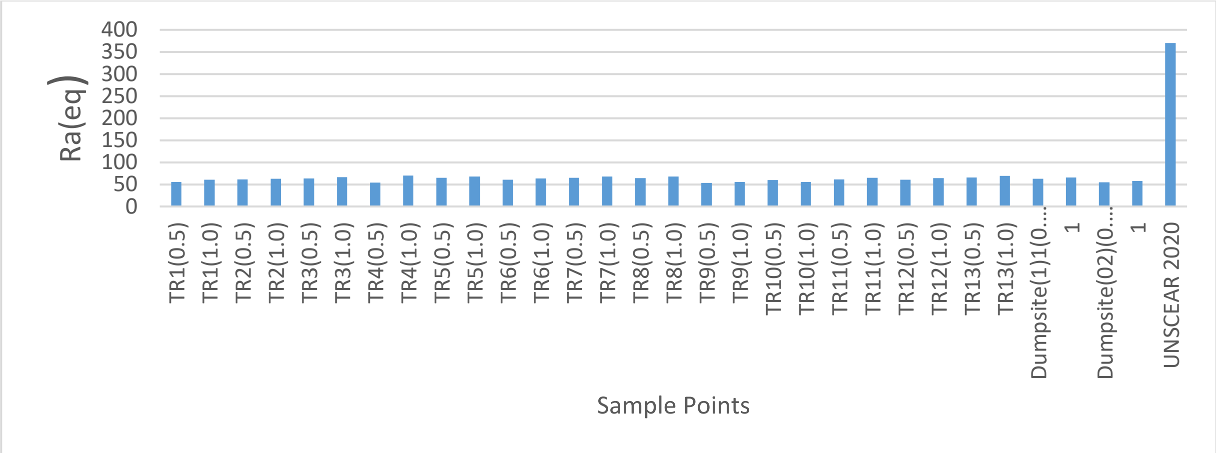

Figure 5: Radium Equivalent Activity VS Sample Points

External annual effective dose equivalent (AEDE_external) ranged from 32.39 μSv yr^{-1} to 43.49 μSv yr^{-1}, with a mean value of 33.93 μSv yr^{-1}. These values are well below the global permissible limit of 70 μSv yr^{-1} for external exposure, suggesting that gamma radiation from surface soils in the area poses negligible radiological risk (Idaho National Laboratory, 2025). Figure 6 also shows the distribution of the external annual effective dose rate across the study area.

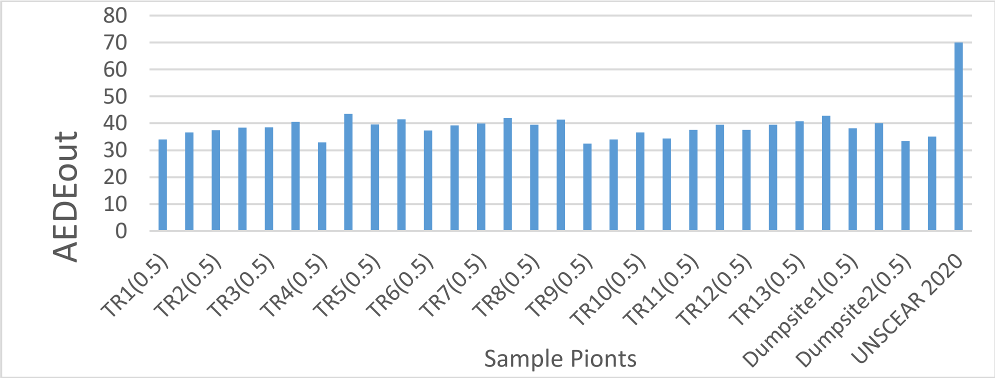

Figure 6: External Annual Effective Dose Equivalent VS Sample Points

Overall, the radiological indices evaluated in this study indicate that the Kurata dumpsite soils present low radiological health risks to residents and workers in the area. However, continuous monitoring is recommended due to the dynamic nature of waste accumulation and potential long-term buildup of radioactive materials.

External Hazard Index (Hex)

The mean external hazard index (Hex) for the analyzed soil samples is 0.150, as shown in Table 4 The calculated external hazard index values range from 0.143 to 0.189. These values are significantly lower than the permissible limit of 1, indicating that gamma radiation emitted from the surface soils does not pose a radiological threat to individuals in the area. The low H(ex) values confirm that external exposure levels remain within internationally accepted safety limits, as recommended by UNSCEAR (2020) and illustrated in Figure 7.

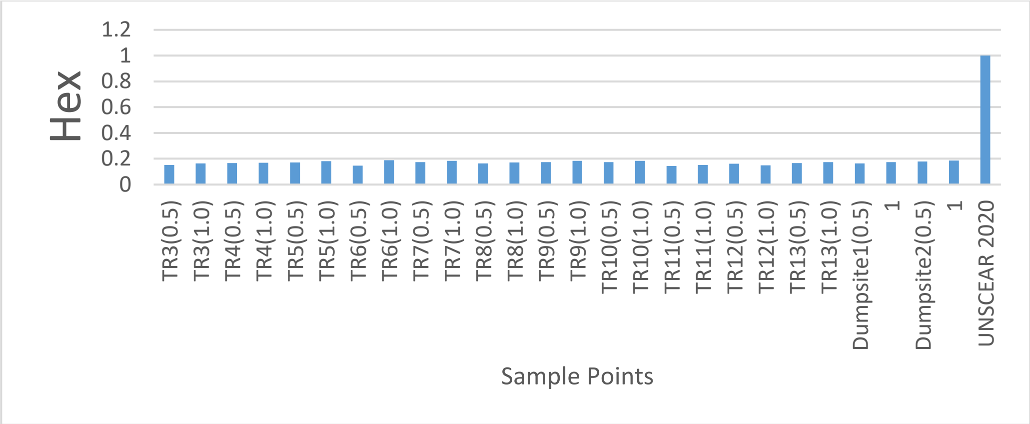

Figure 7: External Hazard Index VS Sample Points

Excess Lifetime Cancer Risk (ELCR)
The excess lifetime cancer risk (ELCR) values calculated for the study area range from 179.95×10^{-6} to 243.67×10^{-6}, with a mean value of 184.95×10^{-6}, as presented in Table 4. The mean ELCR value for the studied samples is therefore 184.95×10^{-6}. These values are below the global average reference value of 0.29×10^{-3}, indicating that the probability of developing cancer due to lifetime exposure to natural background radiation in the area is low. Consequently, the radiological health risk to residents and workers around the study area is considered negligible (Idaho National Laboratory, 2025).

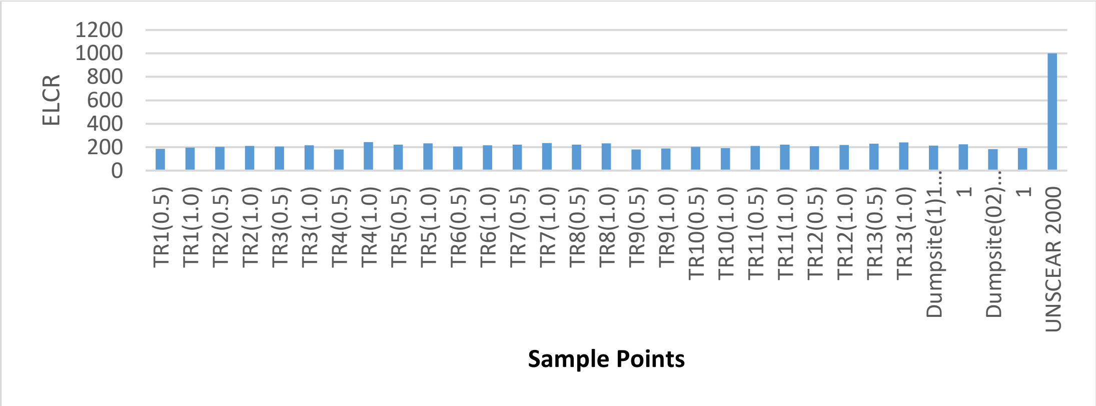

Figure 8: Excess Lifetime Cancer Risk VS Sample Points

Comprehensive analyses of Kurata Soil resistivity and Radioactivity Activity
The relationships appear to be non-linear or affected by outliers. This finding is scientifically significant as it demonstrates the independence of electrical and radiological properties in soils, requiring separate measurement approaches for comprehensive site characterization. The study effectively shows that electrical resistivity cannot serve as a proxy for natural radioactivity levels in soil systems, at least for the conditions studied.
The correlation analysis reveals predominantly weak relationships between topsoil resistivity and the measured radionuclides in the Kurata study area. The moderate positive correlation between topsoil resistivity and K-40 ($r = 0.3616$) suggests some lithological control on both parameters, whereas Ra-226 and Th-232 exhibit weak associations with resistivity (as shown in figures 9 and 10). Overall, the low correlation coefficients indicate that radiological characteristics and geoelectrical properties are controlled by different geological and geochemical processes, highlighting the complexity of subsurface conditions within the study area.

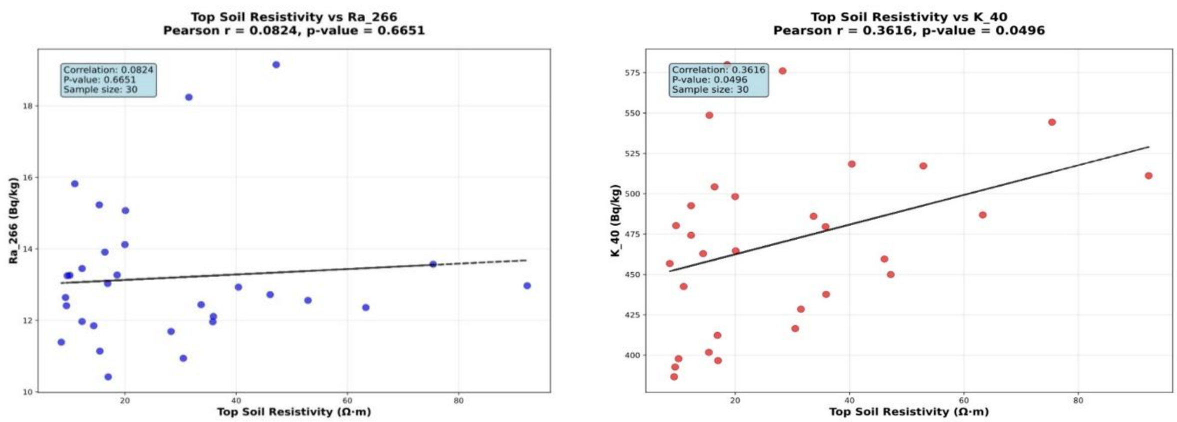

(a) (b)

Figure 9: Kurata Correllation Analyses Results (a) Pearson correlation between topsoil resistivity and Ra-226 (b) Pearson correlation between topsoil resistivity and K-40

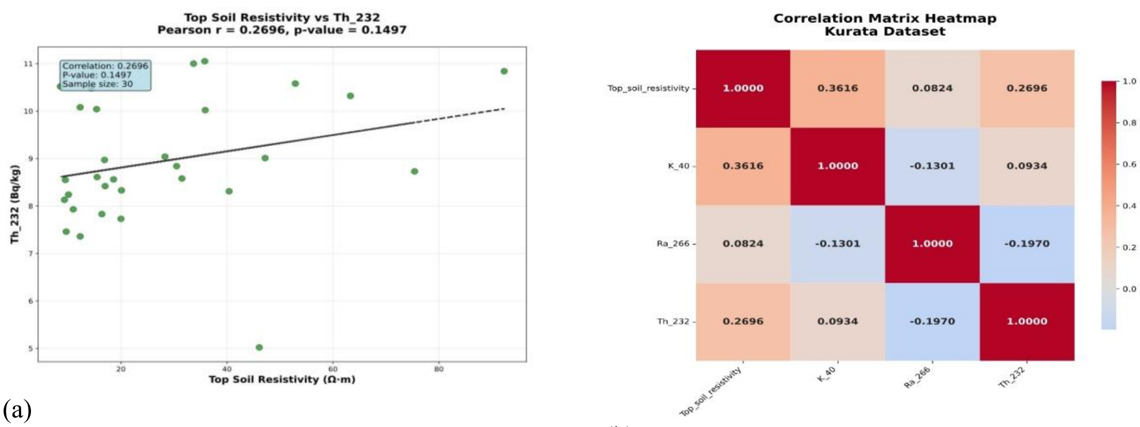

(a) (b)

Figure 10: Kurata Correllation Analyses Results (a) Pearson correlation between topsoil resistivity and Th-232 (b) Correlation matrix heat map

CONCLUSION

Kurata geology appears more stratified with complex layering in some zones. Peat/leachate zones were marked by low resistivity (<15 Ω m). These low-resistivity zones indicate fluid or contaminant percolation, possibly from nearby dumpsites, frequently present within the top 5–10 m. In the layered subsurface in several traverses (e.g., Traverse 2 and Traverse 5), up to six distinct layers were found. High resistivity zones were notable in Traverse 12 and 14, which had values exceeding 5000 Ωm in lateritic sand layers at depth. Topsoil ranged from leachate-contaminated clay to sandy clay. Sand and dry sand were detected with high resistivity (>200 Ωm) deeper in the profiles. Lateritic sand was also found at depths with the highest resistivity values (~1000–3500 Ωm). In some profiles, clay acts as a barrier, but in many cases, the presence of clayey sand and fractured sand indicates potential for vertical and lateral contaminant migration. Sand layers typically show high resistivity and are usually at deeper levels, indicating aquifer potential but also vulnerability if not protected from overlying leachate zones. Lateritic Sand Zones With high resistivity, these appear competent and uncontaminated; however, their depth limits accessibility and use without borehole drilling, the longitudinal conductance value of 0.0169 to 0.9382 mho indicates a poor, weak, and good protective capacity of the Study area.

The evaluation of radiological hazard indices for the studied soil samples indicates that the area is radiologically safe for both residents and workers. The mean external hazard index (H_ex) of 0.150, with values between 0.143 and 0.189, is significantly lower than the permissible limit, indicating that gamma radiation from surface soils does not pose a radiological threat.

Furthermore, the estimated excess lifetime cancer risk (ELCR), which ranged from 179.95×10^{-6} to 243.67×10^{-6} with a mean value of 184.95×10^{-6}, is below the globally accepted reference level. This confirms that the probability of developing cancer due to long-term exposure to natural radionuclides in the study area is minimal. Overall, the radiological parameters assessed

demonstrate that radiation exposure in the area is negligible and within internationally recommended safety limits. However, Kurata Dumpsites are very close to residential area. Building supposed to be located 500m or more from dumpsite to ensure safety of human health and to avoid unnecessary health hazards, periodic monitoring is recommended to ensure that radiological conditions remain safe, especially considering the continuous accumulation of waste materials at the site.
The heatmap indicates that topsoil resistivity is only weakly to moderately related to the radionuclide concentrations in the Kurata area. The strongest association observed is between resistivity and K-40 ($r = 0.3616$), while Ra-226 shows little dependence on resistivity. The generally low correlation coefficients (< 0.4) suggest that radionuclide distribution is influenced by multiple factors such as lithology, weathering processes, mineral composition, and environmental conditions rather than resistivity alone

REFERENCES

Adebayo, A. O., Adewuyi, T. O., & Oladipo, M. O. (2015). Environmental and health implications of solid waste disposal practices in urban areas. *Journal of Environmental Health Research, 25*(2), 45–56.

Adegoke, I. A., Coker, J. O. and Agbasi, O. E.(2013). Hydrogeological Appraisal of basement and sedimentary terrain in Ogun State, Using geoelectrical methods.International journal of advanced geoscience 8(1)95-101

Adewole, A. O. (2009). Electrical resistivity investigation of groundwater contamination around a municipal landfill site. *Journal of Environmental Hydrology, 17*, 1–10.

Adewuyi, T. O., Olofin, E. A., & Adebayo, A. O. (2014). Solid waste management and public health risks in developing countries. *African Journal of Environmental Science and Technology, 8*(7), 407–415.

Akinloye, M. K., & Olomo, J. B. (2005). Measurement of gamma radiation from naturally occurring radionuclides in Nigerian soils and vegetation. *Nigerian Journal of Physics, 17*(1), 23–30.

Ameloko, A. A., & Ayolabi, E. A. (2018). Application of electrical resistivity tomography for landfill leachate investigation. *Environmental Earth Sciences, 77*(8), 1–14. https://doi.org/10.1007/s12665-018-7481-3

Ehirim, C. N., Nwankwo, C. N., & Onyekuru, S. O. (2009). Application of electrical resistivity method in landfill site investigation. *Journal of Applied Sciences and Environmental Management, 13*(4), 63–68.

Fajana, A. O. (2013). Geophysical investigation of waste disposal sites using electrical resistivity techniques. *Environmental Earth Sciences, 69*(6), 1881–1890.

Idaho National Laboratory. (2025). *Radiological dose assessment and environmental radiation guidelines*. U.S. Department of Energy. https://www.inl.gov

Jones, H. A., & Hockey, R. D. (1964). *The geology of part of southwestern Nigeria*. Geological Survey of Nigeria Bulletin No. 31.

Kogbe, C. A. (1976). Geology of Nigeria. In C. A. Kogbe (Ed.), *Geology of Nigeria* (2nd ed., pp. 273–283). Elizabethan Publishing Company.

Kasoga, P. S., Ndontchueng, M. M., & Ramdhani, S. (2015). Assessment of natural radioactivity levels and radiological hazards in the environment. *Radiation Protection Dosimetry, 167*(1–3), 321–327.

Obiora, D. N., Ibuot, J. C., & George, N. J. (2020). Aquifer vulnerability assessment using geoelectric parameters in urban environments.*Environmental Monitoring and Assessment, 192*(3), 1–15.

Omatsola, M. E., & Adegoke, O. S. (1981). Tectonic evolution and Cretaceous stratigraphy of the Dahomey Basin. *Journal of Mining and Geology, 18*(1), 130–137.

Olagunju, A. O., Adeyemo, I. A., & Ojo, O. A. (2017). Integrated geophysical investigation of groundwater contamination around dumpsites. *Journal of African Earth Sciences, 134*, 1–12.

Olubunmi, P. A., Ademola, J. A., & Bello, A. K. (2018). Radiological assessment of soils around municipal dumpsites. *Journal of Radiation Research and Applied Sciences, 11*(4), 295–302.

Raji, W. O., & Adeoye, A. O. (2017). Assessment of leachate contamination using electrical resistivity method around dumpsites. *Journal of Applied Sciences and Environmental Management, 21*(2), 319–326. https://doi.org/10.4314/jasem.v21i2.16

Rahaman, M. A. (1988). *Recent advances in the study of the Basement Complex of Nigeria*. In P. O. Oluyide, W. C. Mbonu, A. E. Ogezi, I. G. Egbuniwe, A. C. Ajibade, & A. C. Umeji (Eds.), *Precambrian Geology of Nigeria* (pp. 11–43). Geological Survey of Nigeria.

Stempvoort, D. R. V., Ewert, L., & Wassenaar, L. I. (1993). Aquifer vulnerability index: A GIS-compatible method for groundwater vulnerability mapping. *Canadian Water Resources Journal, 17*(4), 369–388.

United Nations Scientific Committee on the Effects of Atomic Radiation. (2020). *Sources and effects of ionizing radiation*. United Nations.

Ugwuanyi, J. U., Onah, G. N., & Ezeh, C. C. (2021). Radiological hazard assessment of soils from waste disposal sites. *Journal of Radiation Research and Applied Sciences, 14*(1), 123–131. https://doi.org/10.1080/16878507.2021.1874216

Yusuf, S. A., Ojo, A. O., & Afolayan, J. F. (2019). Protective capacity evaluation of aquifers using geoelectric methods. *Arabian Journal of Geosciences, 12*(18), 1–12.